Philosophical Magazine,
Vol. 00, No. 00, DD Month 200x, 1–13

Physical properties of the body–centred tetragonal $CaPd_2Ge_2$

Ertuğrul Karaca[1], E. Arslan[1], H. M. Tütüncü*[1,2], G. P. Srivastava[3]

[1]Sakarya Üniversitesi, Fen-Edebiyat Fakültesi, Fizik Bölümü, 54187, Adapazarı, Turkey

[2]Sakarya Üniversitesi, Biyomedikal, Manyetik ve Yarıiletken Malzemeler Araştırma Merkezi (BIMAYAM), 54187, Adapazarı, Turkey

[3]School of Physics, University of Exeter, Stocker Road, Exeter EX4 4QL, UK

(Received 00 Month 200x; in final form 00 Month 200x)

We have investigated the structural, elastic, electronic, and lattice dynamical properties of $CaPd_2Ge_2$ in the body-centred tetragonal $ThCr_2Si_2$ structure using a generalized gradient approximation of the density functional theory and the *ab initio* pseudopotential method. The calculated second-order elastic constants indicate that $CaPd_2Ge_2$ is mechanically stable and behaves in a ductile manner. Our electronic results show that the states close to the Fermi level are primarily contributed by Pd d and Ge p orbitals. A detailed analysis of electron–phonon interaction calculations reveals that the mechanism for superconductivity in $CaPd_2Ge_2$ is mainly governed by interactions of Pd d and Ge p electrons around the Fermi level with acoustic phonon modes and low–frequency optical phonon modes, which strongly change $PdGe_4$ tetrahedral bond angles. The values of the average electron–phonon coupling constant and the logarithmic average frequency are calculated to be 0.66 and 77.3 K, respectively. Inserting these values into the Allen–Dynes formula with using an acceptable value of μ^*= 0.13 for the effective Coulomb repulsion parameter, the value of superconducting transition temperature is obtained to be 1.69 K, which is in excellent agreement with its experimental value.

1 Introduction

Recently, $ThCr_2Si_2$–type AT_2X_2 materials (A: an alkaline earth or a lanthanide element; T: a transition metal; X: Si, P, Ge, or As) have received a great deal of attention of the scientific community. This is because these compounds exhibit extraordinary properties such as intermediate valence [1–5], heavy fermion behaviour [6–10], and different magnetic properties [11–16]. Furthermore, superconductivity in pnictide compounds AT_2Pn_2 (A = alkaline earth, T = transition metal, and Pn = pnictogen) has been studied, with the high transition temperature of T_c ∼38K in (Ba,K)Fe_2As_2 attained when the compound was doped with holes [17, 18]. In recent years, iron-free pnictides such as $BaNi_2P_2$ ($T_c \sim 3$ K) [19, 20], $SrNi_2As_2$ ($T_c = 0.6$K) [21], $SrNi_2P_2$($T_c = 1.4$ K) [22, 23], $BaIr_2P_2$ ($T_c = 2.1$ K) [24], $BaRh_2P_2$ ($T_c = 1.0$ K) [24], $CaPd_2As_2$ ($T_c = 1.27$ K) [25], and $SrPd_2As_2$ ($T_c = 0.92$ K) [25] have been synthesized. In these compounds the magnetic metal (Fe) is either replaced by another magnetic metal (Ni) or other transition metals (Rh, Ir, and Pd), and arsenic is totally replaced by other pnictogen–phosphorus.

The discovery of superconductivity in these $ThCr_2Si_2$–type materials has motivated physicists to study their structural and electronic properties. Shein and Ivanovskii have investigated the structural and elec-

* Corresponding author. Email: t utuncu@sakarya.edu.tr

Philosophical Magazine
ISSN 1478-6435 print/ISSN 1478-6443 online
http://www.tandf.co.uk/journals
DOI: 10.1080/1478643YYxxxxxxxx

tronic properties of $SrNi_2As_2$, $BaNi_2As_2$ and $SrNi_2P_2$ by means of the first-principles full potential linearised augmented plane wave (FP-LAPW) [26]. This theoretical work indicated that the electronic states close to the Fermi level are mainly contributed by Ni d states with some admixture of antibonding P (As) p states. The linear response approach [27] has been utilized to study electron–phonon interaction in $BaNi_2As_2$. The results of this theoretical work suggested that this material is a conventional phonon-mediated superconductor. Moreover, the electronic properties of $BaNi_2P_2$ has been investigated by several theoretical groups [28–31]. These theoretical works [28–31] suggested that the density of states at the Fermi level for $BaNi_2P_2$ is dominated by Ni d states with significant admixture of P p states. Very recently, *ab initio* pseudopotential calculations [32] have been made to study the structural, electronic and vibrational properties of $SrPd_2Ge_2$, $SrPd_2As_2$ and $CaPd_2As_2$ crystallizing in the $ThCr_2Si_2$–type body–centred tetragonal structure. The electronic results of this theoretical works [32] indicate that the density of states at the Fermi level is mainly dominated by the strong hybridization of Pd d states and Ge (or As) p states. Furthermore, electron–phonon interaction calculations [32] for these materials with the linear response method suggest that all these compounds are phonon–mediated superconductors with the medium electron–phonon coupling strength.

In 2014, the discovery of $CaPd_2Ge_2$ as a new superconductor with $T_c = 1.69$ K was reported in the experimental work of Anand and co-workers [33]. This material also adopts the $ThCr_2Si_2$–type structure. Due to the existence of the nonmagnetic transition metal Pd, no magnetic order is available to interfere with the superconducting state. In addition to this, this material includes Ge atoms rather that As or P atoms which are toxic and volatile elements, respectively. Thus, this material is a good choice for searching the origin of superconductivity in the $ThCr_2Si_2$–type structure. Moreover, with a study of the physical properties of $CaPd_2Ge_2$ we can examine the effect of the A element on the physical properties of APd_2Ge_2. Furthermore, we can confirm whether the observed superconductivity in such materials is intrinsic of the $PdGe_4$ layer or not.

Although considerable progress has been made in experimental investigations of superconductivity in $CaPd_2Ge_2$, no theoretical results are available for the electronic and lattice dynamical properties of this material. Similarly, electron–phonon interaction in $CaPd_2Ge_2$ has not yet been studied. Thus, we investigate the structural and electronic properties of $CaPd_2Ge_2$ by employing the plane-wave pseudopotential method and the density functional theory [34, 35]. Details of the electronic band structure and the electronic density of states near the Fermi energy are presented and discussed in detail. We have also made *ab initio* linear response calculations of the lattice dynamics and polarization characteristics of zone-centre phonon modes. Furthermore, the linear response method [34, 35] has been used to determine calculate the electron–phonon matrix elements. The Eliashberg spectral function is obtained from the calculated phonon spectrum and the calculated electron–phonon matrix elements. By integrating the Eliashberg spectral function, the average electron–phonon coupling parameter is calculated. Finally, an explanation for the difference in the superconducting transition temperature between the isostructural materials $CaPd_2Ge_2$ and $SrPd_2Ge_2$ [32] has been put forward.

2 Theory

Calculations of the electronic properties and total energy are performed using the Quantum-Espresso package [34, 35] within the framework of density-functional theory (DFT). The electronic exchange correlation energy is estimated according to the generalized gradient approximation (GGA) of

Perdew–Burke–Ernzerhof [36]. Norm–conserving pseudopotentials are employed for a description of interaction between the ionic cores and valence electrons [37]. Single particle wave functions are expanded in a plane–wave basis, with a kinetic energy cutoff of 60 Ry. The Kohn-Sham equations [38] are solved using an iterative conjugate gradient scheme, employing a set of Monkhorst–Pack special $\boldsymbol{k}$ points [39]. The (8×8×8) grid is chosen in order to determine the structural parameters. With this grid, the equilibrium positions are determined with numerical uncertainty of less than 0.01 $\AA$ when all forces are smaller than 0.1 mRyd/a.u. The electronic structure and electronic density of states are calculated by employing the (24×24×24) grid.

Phonon results have been obtained by employing the linear response method [34,35]. This method avoids the use of supercells and allows the calculation of the dynamical matrix at arbitrary $\boldsymbol{q}$ vectors. In this method, the eigenfrequencies and eigenvectors of lattice vibrations are determined within the framework of self-consistent density functional perturbation theory (DFPT) [34, 35]. A static linear response of the valence electrons is considered in terms of the variation of the external potential corresponding to periodic displacements of the atoms in the unit cell. The screening of the electronic system in response to the displacement of the atoms is taken into account in a self consistent manner. Thirteen dynamical matrices are calculated on the (4×4×4) Monkhorst–Pack $\boldsymbol{q}$–point grid, resulting in phonon frequencies converged to within 0.05 THz. Numerical integration of the Brillouin zone is made using the 8×8×8 Monkhorst-Pack **k**-point sampling.

The electron–phonon coupling and the possibility of superconductivity have been studied within the framework of the Migdal-Eliashberg theory [40–43]. Within this theory, the Eliashberg electron–phonon spectral function $\alpha^2\mathrm{F}(\omega)$ is expressed as

$$\alpha^2 F(\omega) = \frac{1}{2\pi N(E_F)} \sum_{\boldsymbol{q}j} \frac{\gamma_{\boldsymbol{q}j}}{\hbar\omega_{\boldsymbol{q}j}} \delta\left(\omega - \omega_{\boldsymbol{q}j}\right), \tag{1}$$

where $N(E_F)$ is the electronic density of states at the Fermi level and $\gamma_{\boldsymbol{q}j}$ is the phonon line–width for phonon mode $\boldsymbol{q}$. When the electron energies around the Fermi level are linear in the range of phonon energies, the phonon line–width is given by Fermi's "golden rule" formula [42, 43]

$$\gamma_{\boldsymbol{q}j} = 2\pi\omega_{\mathbf{q}j} \sum_{\boldsymbol{k}nm} |\mathrm{g}^{\boldsymbol{q}j}_{(\boldsymbol{k}+\mathbf{q})m;\boldsymbol{k}n}|^2 \delta(\varepsilon_{\boldsymbol{k}n} - \varepsilon_F)\delta(\varepsilon_{(\boldsymbol{k}+\boldsymbol{q})m} - \varepsilon_F), \tag{2}$$

where the Dirac delta functions express energy conservation conditions, and g shows the electron–phonon matrix element. The summations in Eqs. 1 and 2 are done using the (24×24×24) Monkhorst–Pack dense mesh of $\boldsymbol{k}$ points in the irreducible part of the Brillouin zone.

The electron–phonon coupling parameter $\lambda_{\boldsymbol{q}j}$ involving a phonon state $\boldsymbol{q}$j can be expressed as [42, 43]

$$\lambda_{qj} = \frac{\gamma_{qj}}{\pi\hbar N(E_F)\omega_{qj}^2}, \tag{3}$$

where N(E_F) is the electronic density of states at the Fermi level. Finally, the average value of the

electron–phonon coupling parameter is given as:

$$\lambda = \sum_{\boldsymbol{q}j} W(q)\lambda_{\boldsymbol{q}j}, \tag{4}$$

where W(q) is the weight of the $\boldsymbol{q}$ mesh point in the first Brillouin zone. The above summation has been carried out by employing the 4×4×4 grid in $\boldsymbol{q}$ space, which corresponds to 13 special $\boldsymbol{q}$ points.

3 Results

3.1 *Structural, Elastic and Electronic Properties*

One of the most common crystal structures found in intermetallic compounds is the $ThCr_2Si_2$-type body-centred tetragonal structure with space group I4/mmm. The intermetallic compound $CaPd_2Ge_2$ adopts this structure, as plotted in Fig. 1(a). The Ca atoms are located in the corner and centre positions of the unit cell. The transition metal Pd atoms occupy the Wyckoff site 4d [(0, 1/2, 1/4), (1/2, 0, 1/4)] and generate two–dimensional square planes. The Ge atoms fill the Wyckoff site 4e [(0, 0, z), (0, 0, -z)]. As the first step of our *ab initio* study, total energy calculations are performed to determine the equilibrium structural parameters for $CaPd_2Ge_2$. Then, around the region of the total energy minimum, the bulk modulus (B) and the equilibrium volume have been determined by fitting the numerical data to Murnaghan's equation of state [44]. The calculated equilibrium lattice parameters (a and c), the internal parameter (z) and the bulk modulus are presented and compared with recent experimental results [33] in Tab. 1. The slight overestimation of structural parameters a and c results from the application of the GGA approximation. Comparing the optimized lattice parameters in Tab. 1 with those measured experimentally [33], we obtained differences of 1.5% and 2.1% for the lattice parameters a and c, respectively. The value of the calculated internal parameter is almost equal to its experimental value of 0.3745 [33]. To our knowledge, there are no experimental results for the value of B.

The structure of $CaPd_2Ge_2$ contains two layers namely, the Pd–Ge and Ca layers which are arranged alternatively along the z–axis (see Fig. 1(a)). The Pd–Ge layers are separated by the Ca layers. The Pd atom is tetrahedrally surrounded by four Ge atoms while the Ge atom coordinates with four basal Pd atoms and one apical Ge atom. The interatomic distance Pd–Ge is 2.532 $\mathring{A}$ which is smaller than the value expected from the summation of the two atomic radii: 1.40 $\mathring{A}$ for Pd and 1.25 $\mathring{A}$ for Ge. This result indicates that the $PdGe_4$ layers include strong covalent Pd–Ge bonds and weaker Pd–Pd interactions while the bonding between Ca and $PdGe_4$ layers is rather ionic. As a consequence, the bonding in this material can be classified as an interplay between covalent, metallic, and ionic characters. The α, β and γ angles in Fig. 1 are good indicators of distortion in the $PdGe_4$ tetrahedra. The values of α, β and γ are found to be 119.66^o, 104.63^o and 75.37^o which compare well with their experimental values of 120.26^o, 104.36^o and 75.64^o [33]. Fig. 1(b) shows the calculated intra-layer electronic charge density along a Ge-Pd line. This confirms covalent bonding between Ge and Pd. The peak in the bond charge density is closer to Pd than Ge, consistent with the fact that Pd is approximately 20% more electronegative than Ge.

The elastic properties of superconducting material must be studied because the long-wavelength phonon spectrum is intimately related to the elastic properties of the material. In this work, the second order elastic constants are described by means of the energy of a lattice strain [45]. For a body–centred tetragonal

material such as $CaPd_2Ge_2$, we have six independent components of second order elastic constants, i.e. C_{11}, C_{12}, C_{13}, C_{33}, C_{44} and C_{66}. The calculated values of these elastic constants for $CaPd_2Ge_2$ are presented in Tab. 1. We note that no experimental or other theoretical results are available for comparison with our results. The requirements of mechanical stability in a tetragonal crystal lead to the following restrictions on the elastic constants [46]:

$$C_{11} > 0, C_{33} > 0, C_{44} > 0 \text{ and } C_{66} > 0 \tag{5}$$

$$C_{11} - C_{12} > 0 \tag{6}$$

$$C_{11} + C_{33} - 2C_{13} > 0 \tag{7}$$

$$2(C_{11} + C_{12}) + C_{33} + 4C_{13} > 0. \tag{8}$$

As can be seen from Tab. 1, the calculated elastic constants satisfy the above criteria, suggesting that the body–centred tetragonal $CaPd_2Ge_2$ is mechanically stable. For tetragonal crystals, there are two Cauchy relations $C_{12} = C_{66}$ and $C_{33} = C_{44}$ [46]. Tab. 1 clearly shows that the calculated elastic constants do not obey these two relations. This indicates that the non-central forces are very important for $CaPd_2Ge_2$ due to its covalent character since these Cauchy relations are strictly satisfied if the atoms interact only with central forces.

Using the Voigt–Reuss–Hill (VRH) averages [47–49], the isotropic bulk modulus (B_{VRH}), the isotropic shear modulus (G_{VRH}), Poisson ratio (ν) and elastic modulus (E) can be calculated from the second order elastic constants:

$$B_V = \frac{2}{9}(C_{11} + C_{12} + 2C_{13} + C_{33}/2) \tag{9}$$

$$B_R = C^2/M \tag{10}$$

$$C^2 = (C_{11} + C_{12})C_{33} - 2C_{13}^2 \tag{11}$$

$$M = C_{11} + C_{12} + 2C_{33} - 4C_{13} \tag{12}$$

$$G_V = (M + 3C_{11} - 3C_{12} + 12C_{44} + 6C_{66})/30 \tag{13}$$

$$G_R = \frac{15}{(18B_V/C^2 + 6(C_{11} - C_{12}) + 6/C_{44} + 3/C_{66})} \tag{14}$$

$$B_H = \frac{B_V + B_R}{2} \tag{15}$$

$$G_H = \frac{G_V + G_R}{2} \tag{16}$$

$$E = \frac{9B_H G_H}{(3B_H + G_H)} \tag{17}$$

$$\nu = \frac{3B_H - E}{6B_H}. \tag{18}$$

The subscripts V, R and H refer to Voigt, Reuss and Hill, respectively. The calculated values of the

isotropic bulk modulus (B_{VRH}), the isotropic shear modulus (G_{VRH}), Poisson ratio (ν) and elastic modulus (E) are presented in Tab. 2. As can be seen from this table, the calculated value of the isotropic bulk modulus (B_{VRH}) is comparable to the bulk modulus (B) value of 83.20 GPa (see Tab. 1) obtained from the Murnaghan's equation of state [44]. The value of the ratio B_H/G_H is found to be 3.00, which is considerably larger than the critical value of 1.75 separating ductile and brittle materials [49], indicating $CaPd_2Ge_2$ behaves in a ductile manner.

The Debye temperature Θ_D is a fundamental attribute of a crystal because it links elastic properties with thermodynamics properties, such as specific heat, melting temperature and vibrational entropy. In this work, Θ_D of $CaPd_2Ge_2$ is computed by using the mean sound velocity V_m and the following expression [50]:

$$\Theta_D = \frac{h}{k}\left(\frac{3n}{4\pi}\frac{N_A\rho}{M}\right)^{1/3} V_m, \tag{19}$$

where k is Boltzmann's constant, h is the Planck's constant, n is the number of atoms in the molecule, N_A Avogadros number, ρ is the density and M is the molecular weight. The mean sound velocity can be given as:

$$V_m = \left[\frac{1}{3}\left(\frac{2}{V_T^3} + \frac{1}{V_L^3}\right)\right]^{-1/3} \tag{20}$$

$$V_T = \left(\frac{G_H}{\rho}\right)^{1/2} \tag{21}$$

$$V_L = \left(\frac{3B_H + 4G_H}{3\rho}\right)^{1/2}, \tag{22}$$

$$\tag{23}$$

where V_T and V_L are transverse and longitudinal sound velocities, respectively. The values of V_T, V_L and V_m are found to be 1993 m/s, 4153 m/s and 2241 m/s, respectively. Inserting the calculated value of V_m into Eq. 19, the value of Θ_D for $CaPd_2Ge_2$ is found to be 248 K which compares well with its experimental value of 259 K [33].

Fig. 2 presents the calculated electronic band structures of $CaPd_2Ge_2$ without and with spin orbit interaction (SOI) along the high symmetry directions in Brillouin zone of body-centred tetragonal lattice. The calculated band structure (see Fig. 2) reveals metallic character for $CaPd_2Ge_2$ with several bands cutting the Fermi level. There are no full potential calculations for the electronic properties of this material. However, our electronic results for $SrPd_2Ge_2$ [32] , $LuNi_2B_2C$ [51] and $BaNi_2P_2$ [52] are in good accordance with available full potential results. Thus, we expect that our electronic results for $CaPd_2Ge_2$ will show good agreement with the future full potential results. Fig. 2 clearly shows the splitting of bands due to SOI, however, remains negligible, in particular at the Fermi level. Thus, we can conclude that the effect of SOI on the studied material can be ignored. The total density of states (DOS) and the partial DOS of each element, broken up into site and angular momentum contributions, are illustrated in Fig. 3. There is a double peak lying between -11.0 and -7.4 eV which has maximum contribution from the s states of Ge atoms. There are two strong peaks at -3.6 and -2.8 eV in the energy window from -5.7 to -1.8 eV, which are composed mainly of Pd d states with a considerable hybridization of Ge p states. This

hybridization is the evidence for a strong covalent interaction between Pd and Ge atoms. The energy range -1.8 eV up to the Fermi level is contributed by the Pd d, Pd p and Ge p states. We can conclude that the valence DOS region of $CaPd_2Ge_2$ is mainly characterized by the states of $PdGe_4$ layers, while Ca d orbitals contribute mainly to energies far above the Fermi level. This result is expected because Ca atoms are in a charged state close to Ca^{2+}. A critical assessment of DOS shows that the bonding nature in $CaPd_2Ge_2$ is a combination of covalent, ionic and metallic bonds.

The bands close to the Fermi level are crucial for governing superconducting properties because Cooper pairs in the BCS theory are constituted by electrons which have energies close to the Fermi level. From our calculations, the total density of states at the Fermi level ($N(E_F)$) for $CaPd_2Ge_2$ amounts to be 2.57 States/eV. The value of $N(E_F)$ plays a considerable role in obtaining superconducting properties because according to the McMillan-Hopfield expression, the electron–phonon coupling constant λ is given as [42, 43];

$$\lambda = \frac{N(E_F) < I^2 >}{M < \omega^2 >}, \tag{24}$$

where M represents the mass of the atoms and $< \omega^2 >$ denotes the average of squared phonon frequencies. Further, $< I^2 >$ represents the Fermi surface average of squared electron–phonon coupling interaction. As can be seen from the above equation, the large value of $N(E_F)$ makes a positive contribution to the value of λ. The contributions from Ca, Pd and Ge atoms to $N(E_F)$ are approximately 7%, 54%, and 39%, respectively. Pd d, Pd p and Ge p states alone contribute 31%, 19% and 37% to $N(E_F)$, respectively. Thus, following the McMillan-Hopfield expression, we can emphasize that the d electrons of Pd atoms and p electrons of Ge atoms have considerable effects on the superconducting properties of $CaPd_2Ge_2$. When SOI is included, the value of $N(E_F)$ is increased from 2.57 States/eV to 2.59 States/eV. Again, this result shows that the effect of SOI on electronic and superconducting properties of $CaPd_2Ge_2$ is very small. We have to mention that a similar observation has been made for $CaIrSi_3$ in our previous work [53], although its structure ($BaNiSn_3$ type) lacks inversion symmetry along the c-axis.

3.2 *Phonons and Electron–Phonon interaction*

The zone-centre optical phonon modes (12 in all) of $CaPd_2Ge_2$ can be classified by the irreducible representation of the point group D_{4h} (4/mmm). As obtained from group theory, the symmetries of the zone-centre optical phonon modes are presented as

$$\Gamma = 2E_u + 2A_{2u} + B_{1g} + 2E_g + A_{1g},$$

where the E modes are doubly degenerate. The frequencies of the zone-centre optical phonon modes are given together with their electron–phonon coupling parameters and their eigen characters in Tab. 3. The E modes arise from the vibrations of related atoms (see Tab. 3) along the $\hat{x}$ and $\hat{y}$ axes, whereas the one-dimensional A and B modes are characterized by the vibrations of related (see Tab. 3) atoms along the $\hat{z}$ axis. The largest contribution to the electron–phonon coupling parameter comes from the lowest E_g phonon mode. This phonon mode arises from the vibrations of Pd and Ge atoms with Ca atoms at rest. This result is expected because the electronic states near the Fermi level are mainly contributed by the Pd d and Ge p states. This vibrational mode dynamically modifies the tetrahedral bond angles in $PdGe_4$, which leads to

an overlap of Pd d and Ge p orbitals. This strong overlap makes the electron–phonon coupling parameter of the lowest E_g phonon mode larger than the corresponding parameter for other phonon modes. A similar observation has been made for $SrPd_2Ge_2$ [32] which is isostructural to $CaPd_2Ge_2$.

For a realistic discussion of the electron–phonon coupling parameter λ, it is necessary to analyze the electron–phonon matrix elements involving phonons of all polarizations throughout the Brillouin zone. We illustrate the results for the phonon dispersion relations in Fig. 4(a) along several symmetry directions and the corresponding phonon density of states in Fig. 4(b). The phonon spectrum extends up to 6.58 THz and all phonon modes have positive frequencies, strongly suggesting that the optimized $CaPd_2Ge_2$ structure is dynamically stable. The phonon spectrum splits into three regions. The three acoustic and six optical bands extend up to 4.64 THz in the first frequency region. The acoustic phonon branches disperse up to 3.78 THz which indicates strong degree of overlap between the acoustic and low–lying optical phonon modes in this frequency region. This strong overlap may lead to the heat–carrying acoustic branches being scattered by the low–lying optical branches, which may decrease phonon contribution to the thermal conductivity of this material. The second frequency region between 4.67 and 6.04 THz is formed by five optical bands which show considerable dispersion like the optical phonon modes in the first frequency region. There is a gap of 0.03 THz between these two regions. There is only one optical phonon band in the third region between 6.28 and 6.58 THz. This region is separated by gap of 0.24 THz from the five dispersive optical phonon bands distributed in the second region. The nature of the phonon spectrum can be more clearly understood by examining the total and partial phonon density of states (see Fig. 4(b)). Strong overlap between Pd and Ge vibrations exist between 0.0 and 2.5 THz due to the strong covalent bonding between these atoms. The contribution of Pd to the phonon modes is strongest between 2.50–3.75 THz. Thus, we can emphasize that Pd and Ge atoms contribute to acoustic phonon branches and low-lying optical phonon branches. Although Ca is the lightest element in this compound, it dominates at intermediate frequencies from 3.75–4.64 THz. Such intermediate frequencies of Ca vibrations can be related to weak bonding forces between this light mass atom and the remaining atoms. On the other hand, Ge dominates at frequencies above 4.67 THz, although its mass is much heavier than the mass of Ca atom. Furthermore, although Pd atoms are the heaviest of three atoms, they make considerable contribution to the phonon bands above 4.67 THz. This observation can be linked to strong bonding forces between Ge and Pd atoms.

In order to obtain numerical values of the contributions of different phonon modes to couple with electrons, and thus to assess which modes have the ability to impress superconductivity in $CaPd_2Ge_2$ most, we have illustrated the Eliashberg spectral function together with the variation of the electron–phonon coupling parameter (λ) with increasing frequency in Fig. 5. The phonon modes below 3.75 THz make the largest contribution to λ within approximately 77%. This is expected because the low frequency phonon modes make a positive contribution to the strength of electron-phonon coupling parameter according to the McMillan-Hopfield expression. In addition to this, electronic states near the Fermi level are mainly contributed by the d orbitals of Pd and the p orbitals of Ge atoms. Thus, we can conclude that the acoustic phonon branches and low–frequency optical phonon branches are more involved in the process of scattering of electrons than high frequency optical phonon branches. By using Eq. 4, the average value is found to be λ=0.66 which suggests that the electron–phonon interaction in this material is of medium strength. With λ calculated, the transition temperature T_c can be obtained from the Allen-Dynes formula [42, 43]:

$$T_c = \frac{\omega_{\ln}}{1.2} \exp\left(-\frac{1.04(1+\lambda)}{\lambda - \mu^*(1+0.62\lambda)}\right), \tag{25}$$

where the logarithmically averaged phonon frequency $\omega_{\ln}$ can be expressed as

$$\omega_{ln} = exp\left(2\lambda^{-1}\int_0^\infty \frac{d\omega}{\omega}\alpha^2F(\omega)ln\omega\right). \quad (26)$$

Inserting the calculated value of λ into Eq. 26, the value of $\omega_{\ln}$ is determined to be 77.3 K. μ^* in Eq. 25 is the screened Coulomb pseudopotential parameter which takes a value between 0.1 and 0.16 [42, 43]. The value of μ^* is chosen to be 0.13 in the experimental work of Anand and co-workers [33]. Thus, following this experimental work [33], we use this value for μ^*. Using the Allen-Dynes formula and taking the value of $\mu^* = 0.13$, we obtain $T_c = 1.69$ K which is is in excellent agreement with its experimental value [33].

Finally, we make a comparison of superconductivity parameters between $CaPd_2Ge_2$ and its isostructural compound $SrPd_2Ge_2$ [32] by analyzing their electronic and phonon structures. This comparison is shown in Tab. 4. Before making any discussion, we have to specify that there are three main factors which influence the value of T_c for BCS-type superconductors. These factors are the electronic DOS at the Fermi level ($N(E_F)$), the logarithmic average phonon frequency (ω_{ln}), and the strength of electron–phonon coupling parameter (λ). With regards to the electronic structures, the replacement of Sr by Ca decreases the value of $N(E_F)$ from 2.70 States/eV to 2.57 States/eV. This change influences the value of λ because it is directly linked to the change in $N(E_F)$ as noted from the McMillan-Hopfield expression. Furthermore, the replacement of Sr by Ca brings down the value of λ from 0.74 to 0.66. These two changes make the value of T_c for $CaPd_2Ge_2$ lower than that of $SrPd_2Ge_2$ [32]. Although Sr is replaced by Ca, superconductivity in $CaPd_2Ge_2$ still exists. Thus, we can conclude that the observed superconductivity in both materials seems to be intrinsic of the $PdGe_4$ layers, whereas A (Sr or Ca) stabilizes their structure by donating electrons to $PdGe_4$ layers. This clearly describes the retention of medium superconductivity in $CaPd_2Ge_2$ upon the replacement of Sr by Ca.

4 Summary and Conclusion

In this work, we have studied the structural, elastic, electronic, lattice dynamical, and electron–phonon interaction properties of $CaPd_2Ge_2$ adopting the $ThCr_2Si_2$–type structure by using the generalized gradient approximation of the density functional theory and the planewave pseudopotential method. The calculated structural parameters accord very well with their experimental values. The calculated second order elastic constants reveal that the body-centred tetragonal $CaPd_2Ge_2$ is mechanically stable and behaves in a ductile manner. The electronic energy band crossing the Fermi level along the Γ–Z direction is very dispersive, revealing metallic nature of the electronic structure of $CaPd_2Ge_2$. The effect of SOI on the electronic properties of $CaPd_2Ge_2$ is very small while the states close to the Fermi level are primarily contributed by Pd d and Ge p orbitals.

Examination of the Eliashberg spectral function reveals that acoustic and low–frequency optical branches are more involved in the process of scattering of electrons rather than high–frequency optical phonon modes. Our calculations show that electron-phonon coupling is capable of supporting the observed superconductivity. The value of average electron–phonon coupling parameter λ is found to be 0.66, indicating that $CaPd_2Ge_2$ is a medium–coupling BCS superconductor. Using the Allen-Dynes modified McMillan equation with the screened Coulomb pseudopotential parameter $\mu^* = 0.13$, the value of superconducting critical temperature is found to be 1.69 K which is in excellent agreement with its experimental value of

1.69 K.

References

[1] P. A. Alekseev, J. -M. Mignot, K. S. Nemkovski, V. N. Lazukov, E. V. Nefeodova, A. P. Menushenkov, A. V. Kuznetsov, R. I. Bewley and A. V. Gribanov, *Spin dynamics of the intermediate-valence compound $EuCu_2Si_2$*, Journal of Experimental and Theoretical Physics 105 (2007), pp. 14–17.

[2] S. Danzenbächer, D. V. Vyalikh, Yu. Kucherenko, A. Kade, C. Laubschat, N. Caroca-Canales, C. Krellner, C. Geibel, A. V. Fedorov, D. S. Dessau, R. Follath, W. Eberhardt, and S. L. Molodtsov, *Hybridization Phenomena in Nearly-Half-Filled f-Shell Electron Systems: Photoemission Study of $EuNi_2P_2$*, Phys. Rev. Lett. 102 (2009), pp. 026403-1–026403-4.

[3] P. Wang, Z. M. Stadnik, J. Zukrowski, B. K. Cho and J. Y. Kim, *Spin-glass ordering and absence of valence fluctuations of Eu in $EuCu_2Si_2$ single crystals*, Phys. Rev. B 82 (2010), pp. 134404-1–134404-7.

[4] Y. Kakehashi and S. Chandra, *Two-state Weiss model for the anomalous thermal expansion in $EuNi_2P_2$*, Physica B., 447 (2014), pp. 19–22.

[5] S. A. Medvedev, P. Naumov, O. Barkalov, C. Shekhar, T. Palasyuk, V. Ksenofontov, G. Wortmann, and C. Felser, *Structure and electrical resistivity of mixed-valent $EuNi_2P_2$ at high pressure*, J. Phys.: Condens. Matter 26 (2014), pp. 1–5.

[6] G. Seyfarth, A. S. Rüetschi, K. Sengupta, A. Georges, D. Jaccard, S. Watanabe, and K. Miyake, *Heavy fermion superconductor $CeCu_2Si_2$ under high pressure: Multiprobing the valence crossover*, Phys. Rev. B 85 (2012), pp. 205105-1– 205105-13.

[7] Y. Hiranaka, Ai. Nakamura, M. Hedo, T. Takeuchi, A. Mori, Y. Hirose, K. Mitamura, K. Sugiyama, M. Hagiwara, T. Nakama, and Y. Önuki, *Heavy Fermion State Based on the Kondo Effect in $EuNi_2P_2$*, J. Phys. Soc. Jpn. 82 (2013), pp. 083708-1–083708-4.

[8] Y. Tsutsumi, K. Machida, and M. Ichioka, *Hidden crossover phenomena in strongly Pauli-limited multiband superconductors: Application to $CeCu_2Si_2$*, Phys. Rev. B 92 (2015), pp. 020502-1–020502-5(R).

[9] H. Ikeda, Michi-To Suzuki, and R. Arita,*Emergent Loop-Nodal s -Wave Superconductivity in $CeCu_2Si_2$: Similarities to the Iron-Based Superconductors*, Phys. Rev. Lett. 114 (2015), pp. 147003-1–147003-5.

[10] M. Enayat, Z. Sun, A. Maldonado, H. Suderow, S. Seiro, C. Geibel, S. Wirth, F. Steglich, and P. Wahl, *Superconducting gap and vortex lattice of the heavy-fermion compound $CeCu_2Si_2$*, Phys. Rev. B 93 (2016), pp. 045123-1–045123-5.

[11] J. An, A. S. Sefat, D. J. Singh, and Mao-Hua Du, *Electronic structure and magnetism in $BaMn_2As_2$ and $BaMn_2Sb_2$*, Phys. Rev. B 79 (2009), pp. 075120-1–075120-6.

[12] D. H. Ryan, J. M. Cadogan, Shenggao Xu, Zhuan Xu, and Guanghan Cao, *Magnetic structure of $EuFe_2P_2$ studied by neutron powder diffraction*, Phys. Rev. B 83 (2011), pp. 132403-1–132403-4.

[13] H. S. Jeevan, Deepa Kasinathan, Helge Rosner, and Philipp Gegenwart, *Interplay of antiferromagnetism, ferromagnetism, and superconductivity in $EuFe_2(As_{1-x}P_x)_2$ single crystals*, Phys. Rev. B 83(2011), pp. 054511-1–054511-6.

[14] S. Nandi, W. T. Jin, Y. Xiao, Y. Su, S. Price, D. K. Shukla, J. Strempfer, H. S. Jeevan, P. Gegenwart, and Th. Brckel, *Coexistence of superconductivity and ferromagnetism in P-doped $EuFe_2As_2$*, Phys. Rev. B 89 (2014), pp. 014512-1–014512-7.

[15] R. E. Baumbach, V. A. Sidorov, X. Lu, N. J. Ghimire, F. Ronning, B. L. Scott, D. J. Williams, E. D. Bauer, and J. D. Thompson, *Suppression of antiferromagnetism by pressure in $CaCo_2P_2$*, Phys. Rev. B 89 (2014), pp. 094408-1–094408-8.

[16] M. Imai, C. Michioka, H. Ueda, and K. Yoshimura, *Static and dynamical magnetic properties of the itinerant ferromagnet $LaCo_2P_2$*, Phys. Rev. B 91 (2015), pp. 184414-1–184414-7.

[17] M. Rotter, M. Tegel, and D. Johrendt, *Superconductivity at 38 K in the Iron Arsenide $(Ba_{1-x}K_x)Fe_2As_2$*, Phys. Rev. Lett. 101 (2008), pp. 107006-1–107006-4.

[18] K. Sasmal, Bing Lv, B. Lorenz, A. M. Guloy, F. Chen, Yu-Yi Xue, and Ching-Wu Chu, *Superconducting Fe-Based Compounds $(A_{1-x}Sr_x)Fe_2As_2$ with A=K and Cs with Transition Temperatures up to 37 K*, Phys. Rev. Lett 101 (2008), pp. 107007-1–107007-4.

[19] T. Mine, H. Yanagi, T. Kamiya, Y. Kamihara, M. Hirano, and H. Hosono, *Nickel-based phosphide superconductor with infinite-layer structure, $BaNi_2P_2$*, Solid State Commun. 147 (2008), pp. 111–113.

[20] Y. Tomioka, S. Ishida, M. Nakajima, T. Ito, H. Kito, A. Iyo, H. Eisaki, and S. Uchida, *Three-dimensional nature of normal and superconducting states in $BaNi_2P_2$ single crystals with the $ThCr_2Si_2$-type structure*, Phys. Rev. B 79 (2009), pp. 132506-1–132506-4.

[21] E. D. Bauer, F. Ronning, B. L. Scott, and J. D. Thompson, *Superconductivity in $SrNi_2As_2$ single crystals*, Phys. Rev. B 78 (2008), pp. 172504-1–172504-3.

[22] F. Ronning, E. Bauer, T. Park, S.-H. Baek, H. Sakai, and J. Thompson, *Superconductivity and the effects of pressure and structure in single-crystalline $SrNi_2P_2$*, Phys. Rev. B 79 (2009), pp. 134507-1–134507-7.

[23] N. Kurita, F. Ronning, C. F. Miclea, E. D. Bauer, K. Gofryk, J. D. Thompson, and R. Movshovich, *Fully gapped superconductivity in SrNi2P2* , Phys. Rev. B 83 (2011), pp. 094527-1–094527-7.

[24] N. Berry, C. Capan, G. Seyfarth, A. D. Bianchi, J. Ziller, and Z. Fisk, *Superconductivity without Fe or Ni in the phosphides $BaIr_2P_2$ and $BaRh_2P_2$*, Phys. Rev. B 79 (2009), pp. 180502-1–180502-4.

[25] V. K. Anand, H. Kim, M. A. Tanatar, R. Prozorov, and D. C. Johnston, *Superconducting and normal-state properties of APd_2As_2 (A=Ca, Sr, Ba) single crystals*, Phys. Rev. B 87 (2013), pp.224510-1–224510-22.

[26] I. R. Shein and A. L. Ivanovskii, *Electronic and structural properties of low-temperature superconductors and ternary pnictides ANi_2Pn_2 (A=Sr,Ba and Pn=P,As)*, Phys. Rev. B 79 (2009), pp. 054510-1–054510-7.

[27] A. Subedi and D. J. Singh, *Density functional study of $BaNi_2As_2$: Electronic structure, phonons, and electron-phonon superconductivity*, Phys. Rev. B 78 (2008), pp. 132511-1–132511-4.

[28] I.B. Shameem Banu, M. Rajagopalan, Mohammed Yousuf, P. Shenbagaraman, *Electronic and bonding properties of ANi_2P_2 (A=Ca, Sr, Ba)*, J. Alloys Compd. 288 (1999), pp. 88–95.

[29] T. Terashima, M. Kimata, H. Satsukawa, A. Harada, K. Hazama, M. Imai, S. Uji, H. Kito, A. Iyo, H. Eisaki, and H. Harima, *Fermi Surface in $BaNi_2P_2$*, J.Phys.Soc.Jpn. 78 (2009), pp. 033706-1–033706-4 .

[30] I.R. Shein, A.L. Ivanovskii, *Electronic and structural properties of low-temperature superconductors and ternary pnictides ANi_2Pn_2 (A=Sr,Ba and Pn=P,As)*, Phys. Rev. B 79 (2009), pp. 054510-1–054510-7.

[31] D.S. Jayalakshmi and M. Sundareswari, *A comparative density functional study of newly proposed 122 compounds with their parent low-temperature superconductors*, Indian J. Phys. 89 (2015) pp. 201–208.

[32] Ertuğrul Karaca, H. M. Tütüncü, H. Y. Uzunok, G. P. Srivastava, and Ş. Uğur, *Theoretical investigation of superconductivity in $SrPd_2Ge_2$, $SrPd_2As_2$, and $CaPd_2As_2$*, Phys. Rev. B 93 (2016) pp. 054506-1–054506-11.

[33] V. K. Anand, H. Kim, M. A. Tanatar, R. Prozorov, and D. C. Johnston, *Superconductivity and physical properties of $CaPd_2Ge_2$ single crystals*, J. Phys.:Condes. Matter 26 (2014) pp. 405702-1– 405702-11.

[34] R. Bauer, A. Schmid, P. Pavone, and D. Strauch, *Electron-phonon coupling in the metallic elements Al, Au, Na, and Nb: A first-principles study*, Phys. Rev. B 57 (1998) pp. 11276-1–11276-7.

[35] P. Giannozzi, S. Baroni, N. Bonini, M. Calandra, R. Car, C. Cavazzoni, D. Ceresoli, G. L. Chiarotti, M. Cococcioni, I. Dabo, A.D. Corso, S. de Gironcoli, S. Fabris, G. Fratesi, R. Gebauer, U. Gerstmann, C. Gougoussis, A. Kokalj, M. Lazzeri, L. Martin-Samos, N. Marzari, F. Mauri, R. Mazzarello, S. Paolini, A. Pasquarello, L. Paulatto, C. Sbraccia, S. Scandolo, G. Sclauzero, A.P. Seitsonen, A. Smogunov, P. Umari and R.M. Wentzcovitch, *QUANTUM ESPRESSO: A modular and open-source software project for quantum simulations of materials*, J. Phys.: Condens. Matter 21 (2009) pp. 395502-1– 395502-19.

[36] J. P. Perdew, K. Burke, and M. Erzerhof, *Generalized gradient approximation made simple*, Phys. Rev. Lett. 77 (1996) pp. 3865–3868.

[37] R. Stumpf, X. Gonze and M. Scheffler, *A List of Separable, Norm-conserving, Ab Initio Pseudopotentials* Fritz-Haber-Institut, Berlin, 1990.

[38] W. Kohn and L. J. Sham, *Self-consistent equations including exchange and correlation effects*,Phys. Rev. 140 (1965) pp. A1133–A1138.

[39] H. J. Monkhorst and J. D. Pack, *Special points for brillonin-zone integrations*, Phys. Rev. B 13 (1976) pp. 5188–5192.

[40] A. B. Migdal,*Interaction between Electrons and Lattice Vibrations in a normal metal* Zh. Eksp. Teor. Fiz., 34 (1958) pp. 996–1001.

[41] G. M. Eliashberg,*Interactions between Electrons and Lattice Vibrations in a Superconductor*, Sov. Phys. JETP., 11 (1960) pp.696–702.

[42] P. B. Allen, *Neutron spectroscopy of superconductors*, Phys. Rev. B 6 (1972) pp. 2577–2579.

[43] P. B. Allen and R. C. Dynes, *Transition temperature of strong-coupled superconductors reanalyzed*, Phys. Rev. B 12 (1975) pp. 905–922.

[44] F. D. Murnaghan, *The compressibility of media under extreme pressures*, Proc. Nat. Acad. Sci. USA 30 (1944) pp. 244–247.

[45] M. J. Mehl, J. E. Osburn, D. A. Papaconstantopoulos, and B. M. Klein, *Structural properties of ordered high-melting-temperature intermetallic alloys from first-principles total-energy calculations*, Phys. Rev. B 41 (1990) pp. 10311–10323.

[46] M. Born, K. Huang, *Dynamical Theory of Crystal Lattices*, Clarendon, Oxford (1956).

[47] W. Voigt, *Lehrbuch der Kristallphysik*, Leipzig, Taubner, (1928).

[48] A. Reuss, *Berechnung der Fliegrenze von Mischkristallen auf Grund der Plastizittsbedingung fr Einkristalle*, Z. Angew. Math. Mech. 9 (1929) pp. 49–58.

[49] R. Hill, *The Elastic Behaviour of a Crystalline Aggregate*, Proc Phys Soc London A 65 (1952) pp. 349–354.

[50] O. L. Anderson,*A simplified method for calculating the Debye temperature from elastic constants*, J Phys Chem Solids, 24 (1963), pp. 909–917.

[51] H. M. Tütüncü, H. Y. Uzunok, Ertuğrul Karaca, G. P. Srivastava, S. Özer, and Ş. Uğur, *Ab initio investigation of BCS-type superconductivity in LuNi2B2C–type superconductors*,Phys. Rev. B 92 (2016), pp.054510-1–054510-17.

[52] Ertuğrul Karaca, H. M. Tütüncü, G. P. Srivastava, and Ş. Uğur, *Electron–phonon superconductivity in the ternary phosphides BaM_2P_2 (M=Ni,Rh,and Ir)*,Phys. Rev. B 94 (2016), pp.054507-1–054507-11.

[53] H.Y. Uzunok, E. İpsara, H.M. Tütüncü, G.P. Srivastava, A. Başoğlu *The effect of spin orbit interaction for superconductivity in the noncentrosymmetric superconductor $CaIrSi_3$*, J. Alloys Compd. 681 (2016), pp.205–211.

Table 1. The calculated structural parameters and second order elastic constants (C_{ij}) for the body–centred tetragonal $CaPd_2Ge_2$, and their comparison with recent experimental results. The lattice parameters are given in $\mathring{A}$ while the bulk modulus and second order elastic constants are given in GPa.

Source	a	c	z	B	C_{11}	C_{12}	C_{13}	C_{33}	C_{44}	C_{66}
This work	4.3776	10.1823	0.3749	83.20	127.91	40.53	66.13	132.32	30.54	12.81
Experimental [33]	4.3116	9.9675	0.3745							

Table 2. Isotropic bulk modulus B_{VRH}, shear modulus G_{VRH}, Young's modulus E (all in GPa) and Poisons's ratio ν for $GaPd_2Ge_2$, determined from the corresponding second order elastic constants C_{ij}

Source	B_V	B_R	B_H	G_V	G_R	G_H	E	ν
This work	81.52	80.34	80.93	29.14	24.68	26.91	72.67	0.35

Table 3. Calculated zone-centre optical phonon mode frequencies (ν), electron–phonon coupling parameters (λ) and phonon eigen characters for the body–centered tetragonal $CaPd_2Ge_2$.

Mode	E_g	B_{1g}	E_u	A_{2u}	A_{2u}	E_u	E_g	A_{1g}
ν (in THz)	2.024	3.105	4.100	4.621	5.258	5.856	5.869	6.452
λ	0.103	0.084	0.007	0.006	0.006	0.005	0.025	0.079
Eigen characters	Pd+Ge	Pd	Ca+Pd	Ca+Ge	Ge+Pd+Ca	Ge+Pd+Ca	Ge+Pd	Ge

Table 4. Comparison of superconducting state parameters for $CaPd_2Ge_2$ and $SrPd_2Ge_2$. Theoretical results for $SrPd_2Ge_2$ are taken from Ref. [32].

Material	$N(E_F)$(States/eV)	ω_{ln}(K)	λ	T_c(K)
$CaPd_2Ge_2$	2.57	77.3	0.66	1.69
$SrPd_2Ge_2$ [32]	2.70	101.4	0.740	3.20

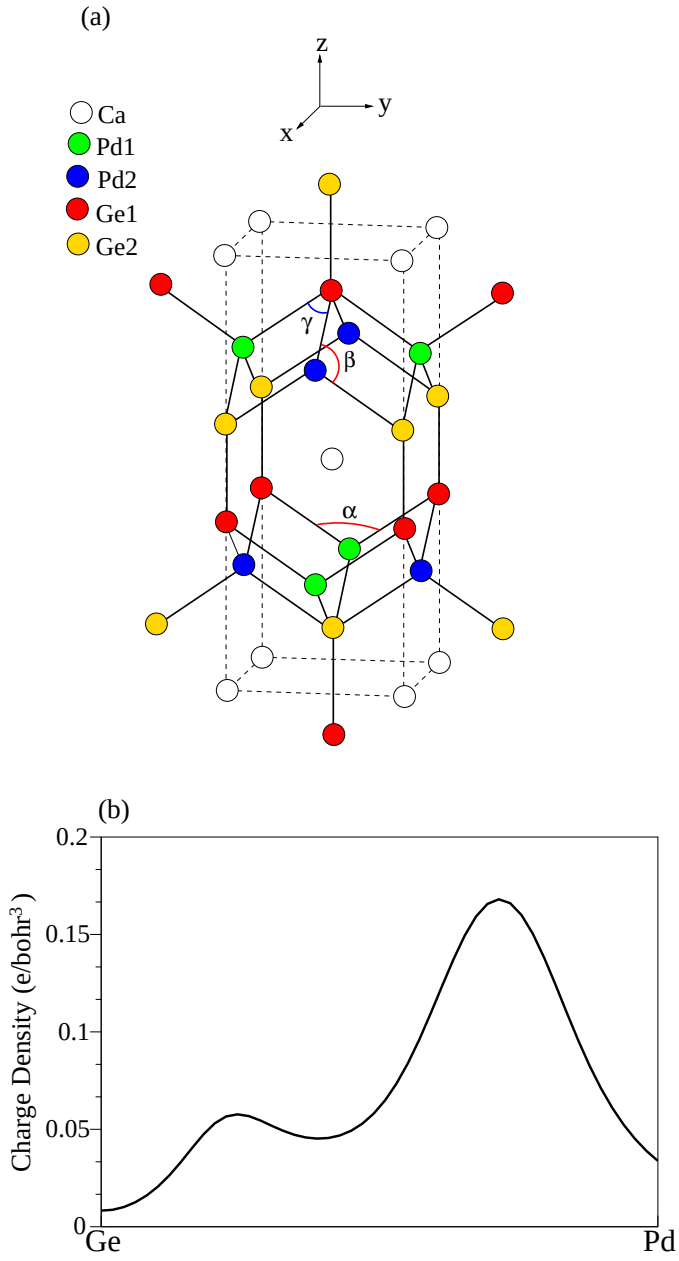

Figure 1. (a) The $ThCr_2Si_2$-type crystal structure of $CaPd_2Ge_2$. (b) The covalent nature of the intra-layer electronic charge density between Ge and Pd atoms is shown.

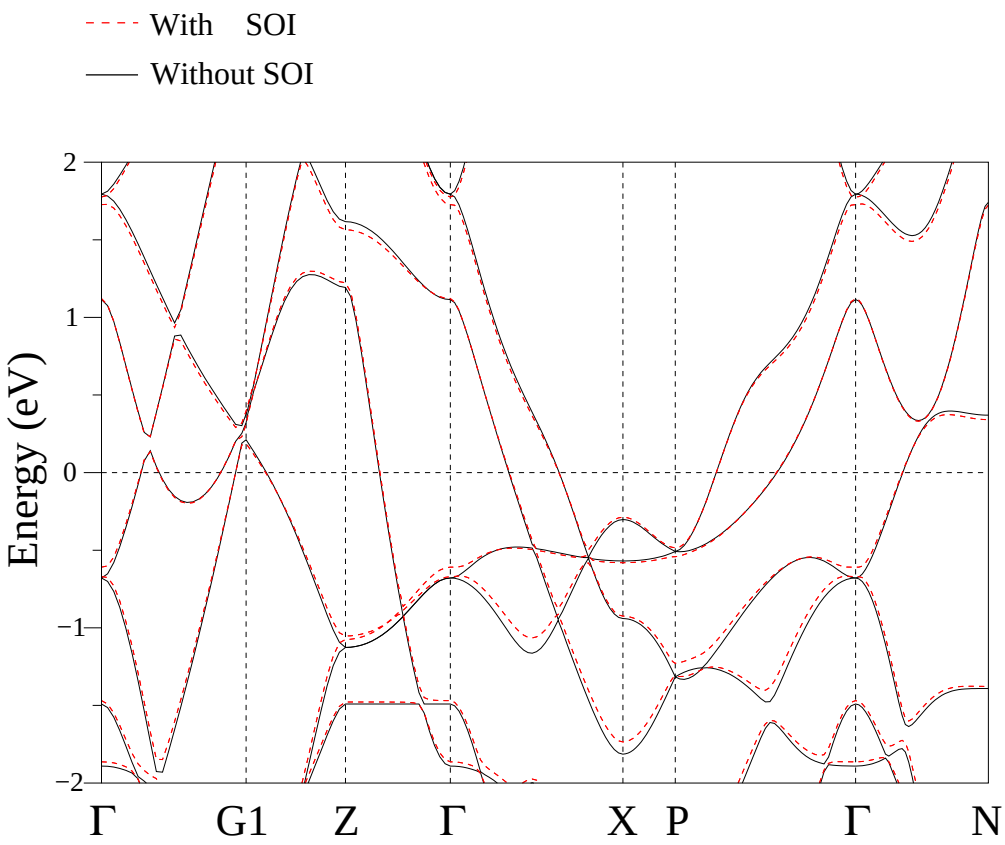

Figure 2. The electronic band structure with and without spin orbit interaction (SOI) for $CaPd_2Ge_2$ in the $ThCr_2Si_2$ crystal structure. The Fermi level corresponds to 0 eV. The high–symmetry points in the irreducible Brillouin zone in cartesian coordinates are: G1= $\frac{2\pi}{a}((\frac{1}{2}+\frac{a^2}{2c^2})$, 0.00, 0.00), Z = $\frac{2\pi}{a}$(0.00,0.00,$\frac{a}{c}$), X= $\frac{2\pi}{a}$(0.50,0.50,0.00), P= $\frac{2\pi}{a}$(0.50,0.50,$\frac{a}{2c}$), and N= $\frac{2\pi}{a}$(0.0,0.50,$\frac{a}{2c}$). Note that G1 is the zone boundary in the [100] direction.

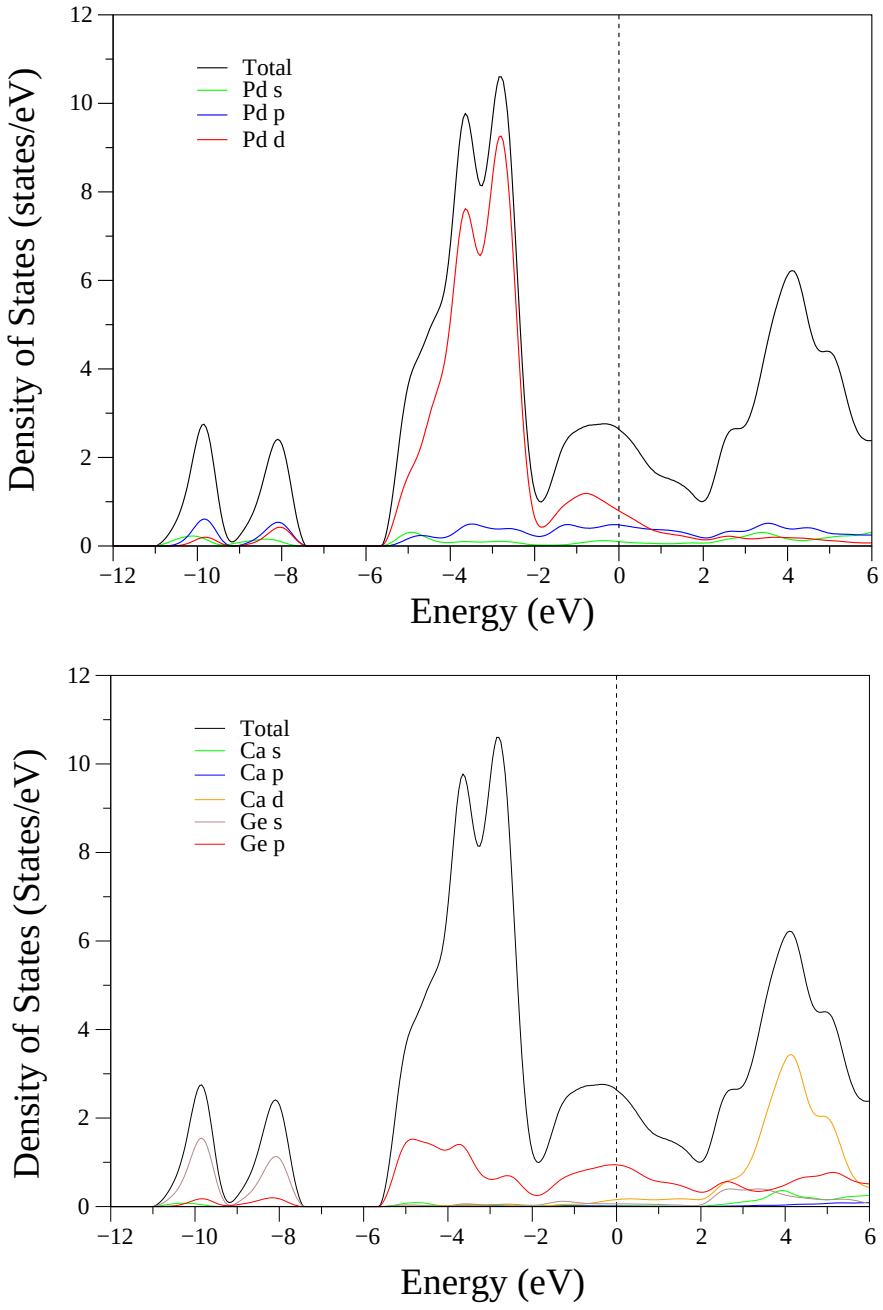

Figure 3. The total and partial density of states for $CaPd_2Ge_2$ in the $ThCr_2Si_2$ crystal structure.

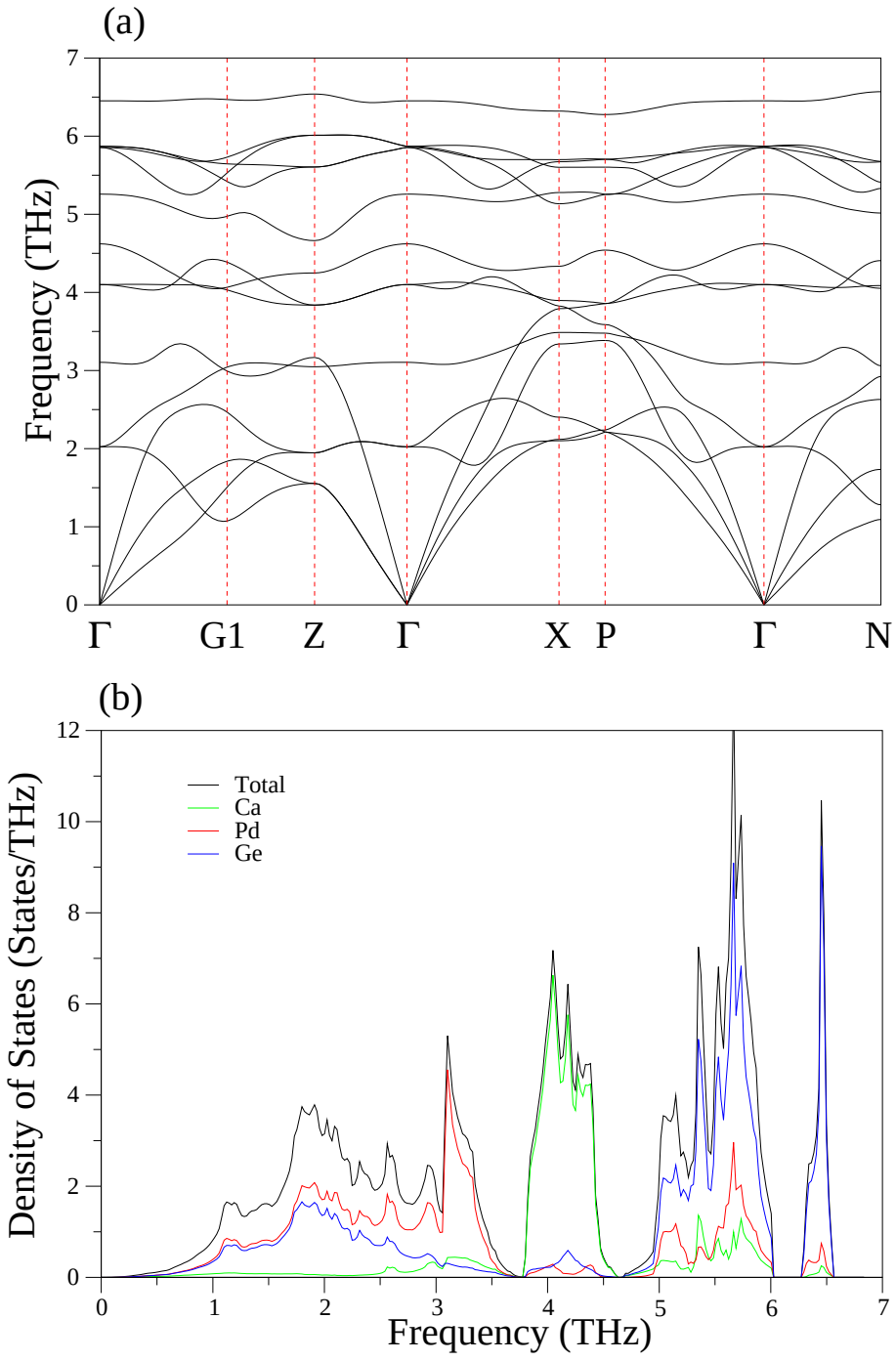

Figure 4. (a) The calculated phonon dispersion relations for the body–centered tetragonal $CaPd_2Ge_2$ along symmetry directions of the body–centered tetragonal Brillouin zone. (b) Total and partial phonon density of states.

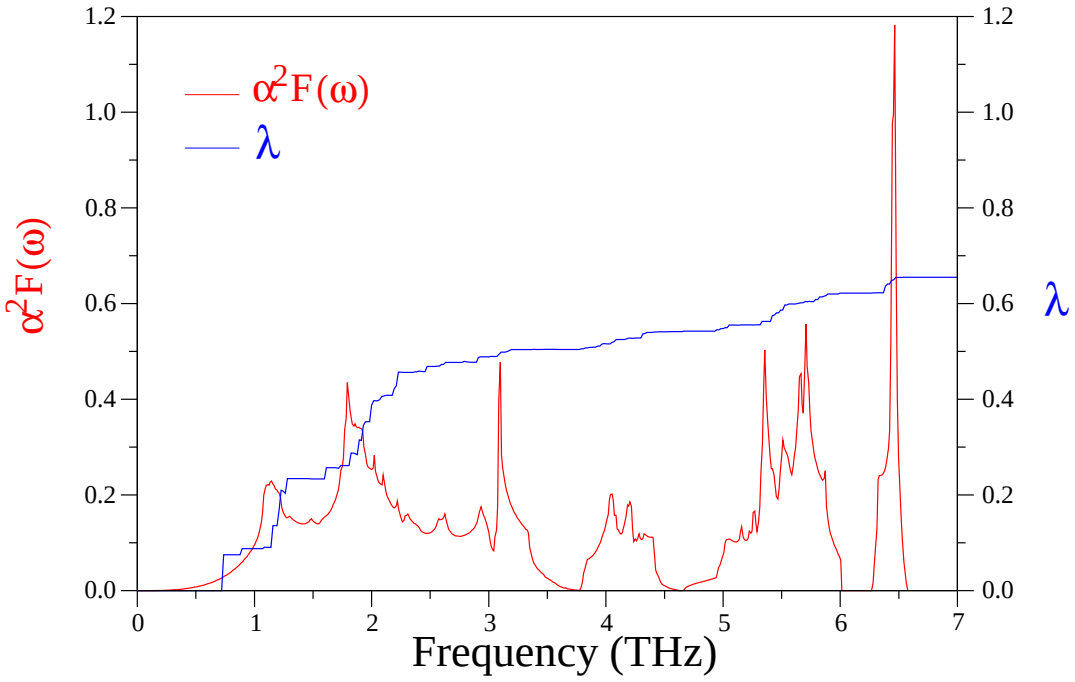

Figure 5. The calculated electron–phonon spectral function $\alpha^2F(\omega)$ (red line) and the variation of the electron–phonon coupling parameter (blue line) with rising frequency for $CaPd_2Ge_2$.